Journal of *Marine Science and Engineering*

MDPI

Article

Atmospheric Drivers of Oceanic North Swells in the Eastern Caribbean

Timothy W. Hawkins [1,*], Isabelle Gouirand [2], Theodore Allen [3] and Ali Belmadani [4]

[1] Department of Geography and Earth Science, Shippensburg University, Shippensburg, PA 17257, USA
[2] Department of Physics, Cave Hill Campus, The University of the West Indies, Cave Hill, St. Michael BB11000, Barbados; isabelle.gouirand@cavehill.uwi.edu
[3] Caribbean Institute for Meteorology and Hydrology, St. Husbands BB23006, Barbados; tallen@cimh.edu.bb
[4] Météo-France, Direction Interrégionale Antilles-Guyane, 97200 Fort-de-France, Martinique, France; ali.belmadani@meteo.fr
* Correspondence: twhawk@ship.edu

Abstract: Large wintertime ocean swells in the Caribbean, known as north swells, generate high surf and expose communities, ecosystems, and infrastructure to hazardous conditions. Empirical orthogonal functions and cluster analyses using ERA5 reanalysis swell data are performed to characterize north swells in the eastern Caribbean and to establish a ranked list of historical events. ERA5 atmospheric and swell data are used to create basin-scale sea-level pressure, surface wind and swell composites for north swell events of different magnitudes. Additionally, storm events are identified in the mid-latitude North Atlantic Ocean. North swells are predominantly generated by storms that intensify off the North American east coast. However, there is a subset of moderately sized swells associated with a westward-located high-pressure system in the North Atlantic. While lower sea-level pressure and stronger surface winds are important for generating larger swells, the location of the low-pressure center and storm track as well the zonal speed of the storm are critical in the development of large eastern Caribbean north swells. The largest such events are associated with storms located comparatively further southeast, with a more zonal trajectory, and slower zonal speed. Large storms located further northwest, with a more southwest to northeast trajectory, and faster zonal speeds are associated with weaker north swells or in many cases, no significant north swell in the eastern Caribbean.

Keywords: ocean swell; mid-latitude cyclone; storm track; Caribbean; North Atlantic; reanalysis

Citation: Hawkins, T.W.; Gouirand, I.; Allen, T.; Belmadani, A. Atmospheric Drivers of Oceanic North Swells in the Eastern Caribbean. *J. Mar. Sci. Eng.* **2022**, *10*, 183. https://doi.org/10.3390/jmse10020183

Academic Editor: Alfredo L. Aretxabaleta

Received: 31 December 2021
Accepted: 27 January 2022
Published: 29 January 2022

1. Introduction

Wind-generated surface ocean waves are an illustration of the atmospheric forcing on the ocean, where steady surface winds drive wave growth and subsequent swell propagation across the ocean (e.g., [1]). The North Atlantic wave climate has the largest seasonal variation among ocean sub-basins, which results from a combination of highly variable seasonal wind forcing and Atlantic basin geometry that prevents the penetration of year-round Southern Ocean swells [2–4]. The largest (smallest) wave heights and periods are observed in winter (summer) due to increased (decreased) average westerly wind intensity [2]. Climatological wind intensity is modulated by the meridional pressure gradient between the subtropical anticyclone and the subpolar low, the pressure gradient itself being driven by the temperature gradient between the tropics and high latitudes, which peaks in boreal winter.

While the atmospheric processes that drive ocean waves are mostly restricted to specific latitudinal bands within the North Atlantic sub-basin (e.g., mid-latitude storm tracks, easterly trade winds, and tropical cyclones), waves can propagate over long distances and in various directions in the form of energetic, long-period swell (e.g., [5]). In particular, boreal wintertime mid-latitude storm activity to the east of the North American continent

occasionally triggers large waves that can travel as far east as the European and West African coasts, and as far south as the Eastern Caribbean islands and South American shorelines [6,7], where they represent a hazard to coastal populations and can cause significant damage to coastal ecosystems and infrastructure [8,9]. This hazard may be further amplified in the future as small island states, such as the Caribbean islands, are especially vulnerable to climate change-driven marine hazards such as sea level rise, changes in tropical cyclone activity, and increasing North Atlantic wave heights [10–12]. Indeed, the climate and topography of the Caribbean islands have favoured the development of social and economic activities that strongly rely on tourism along the exposed coastal area. Despite notable improvements in the prediction, management, and mitigation policies of both present and future marine hazards, most of the literature focuses on extreme waves caused by tropical cyclones (e.g., [11,13–15]). Few published works are dedicated to understanding extreme wave climatology of extratropical origin in the Caribbean region (e.g., [16]).

A few case studies of swell propagation from distant sources have been conducted for the Caribbean [9], most of them focusing on the March 2008 extreme swell event [6–8]. This event resulted from a deep low-pressure system located offshore of the North American east coast (Figure 1). Jury (2018) suggests similar atmospheric conditions drive other major such north swell events in the Caribbean islands, consistent with dominant wintertime northerly swell direction in the tropics and despite the year-long presence of easterly trade winds [2]. A more systematic attribution of the characteristics of the atmospheric drivers of such events is, however, lacking.

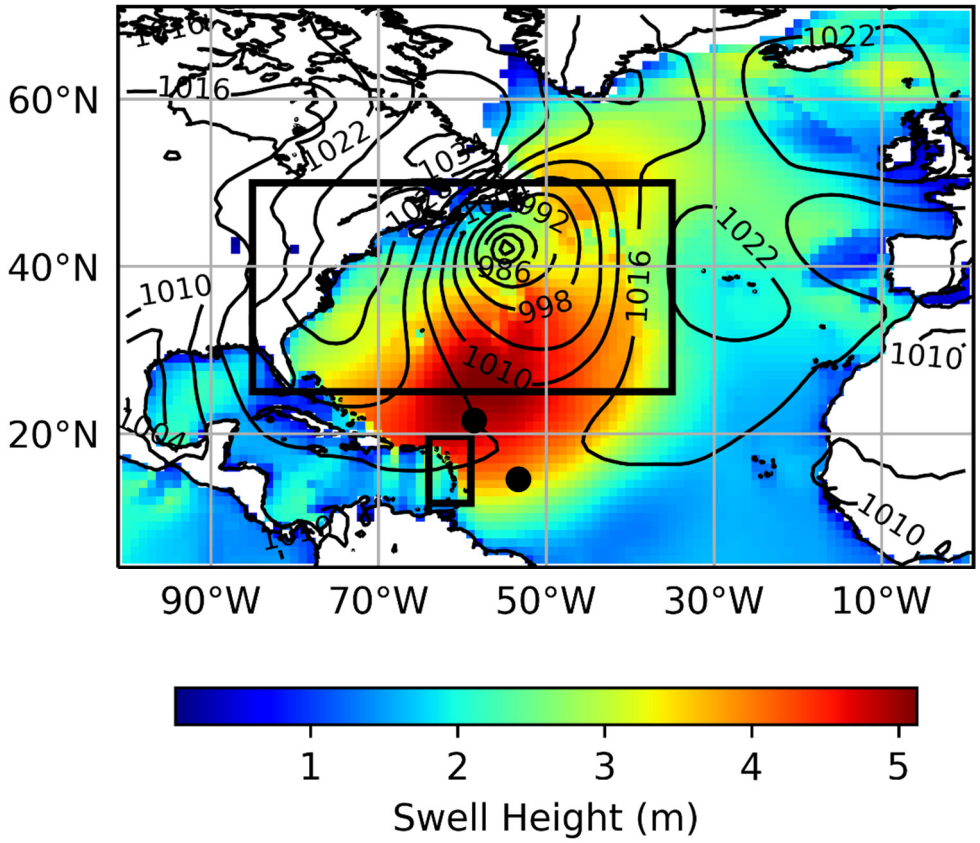

Figure 1. Study area and atmospheric and ocean swell conditions from the ERA5 reanalysis during the largest north swell event in the analysis. The map bounding box is the area for which composite maps are created. The large rectangle is the area for which storms are identified while the small rectangle is the eastern Caribbean north swell study area. Circles are NOAA buoys 41040 (14.5° N, 53.3° W) and 41044 (21.6° N, 58.6° W). Shading indicates swell height on 20 March 2008, the highest day of the highest swell event during the study period (see Table S1), and contours indicate sea level pressure, with a 6 hPa interval, two days prior on 18 March 2008.

The present study, therefore, focuses on these wintertime north swell events, propagating southward and reaching the Lesser Antilles, to further understand the atmospheric conditions that generate them, based on a global coupled atmospheric/wave reanalysis. The main objectives consist of (i) identifying historical north swell events that reached the eastern Caribbean based on swell height, period, and direction; (ii) determining the mid-latitude synoptic atmospheric patterns that generate these events; and (iii) assessing why some synoptic events generate waves that affect the eastern Caribbean, while other synoptic events mostly affect other parts of the sub-basin (e.g., eastern boundaries). Investigating these objectives is important, not only for the short-term anticipation of coastal hazards and the improvement of operational early warning systems, but also for the assessment of future hazards in the region in relation to projected changes in weather and climate patterns [15,17]. Section 2 of the paper identifies the study region and describes the data used to address the above objectives, followed by a detailed description of the methods used to identify and characterize swell events and the associated distant storms. The results are given in Section 3 and discussed in Section 4.

2. Materials and Methods

2.1. Study Area

The map boundary (5° N–70° N, 0° E–100° W) (Figure 1) shows the full study area for which atmosphere and swell composite maps are created (see Section 2.5). The large internal rectangle (25° N–50° N, 35° W–85° W) is the area in which synoptic atmospheric systems are examined (Section 2.6), and the small internal rectangle (11.7° N–19.7° N, 59° W–64° W) is the area in which the north swell is examined for the eastern Caribbean (Section 2.4).

2.2. ERA5 Reanalysis

Swell and atmospheric variables derived from hourly ERA5 reanalysis data [18,19] are obtained from the Copernicus Climate Change Service (C3S) climate data store (https://cds.climate.copernicus.eu/cdsapp#!/home (accessed on 19 January 2021)) for "significant height of total swell", "mean period of total swell", "mean direction of total swell", "mean sea level pressure" and, "10 m u and v components of wind" from the 40 November to April (NDJFMA) periods within the November 1979 to April 2019 record. From this point forward, variables are referred to by the following short names: swell height, swell period, swell direction, sea level pressure, surface wind speed, and surface wind direction. Data resolution is 0.5° for the swell variables within the eastern Caribbean study area and 1° for swell and atmospheric variables within the full study area (Figure 1). Both 0.5° and 1° data are obtained directly from the C3S climate data store.

Daily averages are computed for all variables. For swell direction, hourly values are decomposed into zonal and meridional (x and y) components before averaging. Unity magnitude is used as swell direction is derived from wave energy spectra and therefore lacks an explicit associated magnitude, unlike surface wind vectors. For consistency, surface wind u and v components are normalized by wind speed. Finally, the resulting average x/y and u/v components are used to calculate average daily swell and wind directions.

2.3. NOAA Buoys

Two wave buoys located near the eastern Caribbean study area (Figure 1) are chosen to validate the use of daily ERA5 gridded reanalysis swell data. NOAA buoys 41040 and 41044 are both spectral wave buoys and partition wave energy into swell and wind sea categories. Daily averages are calculated from sub-daily data. Buoy observations begin in 2005 and 2009, resulting in periods of record of 14 and 10 NDJFMA seasons, for buoys 41040 and 41044 respectively. Additionally, buoys 41040 and 41044 are missing 515 of 2537 days (20%) and 141 of 1812 days (8%), respectively. Along with the scarce buoy spatial distribution and comparatively shorter records, these limits suggest the use of ERA 5 reanalysis data is preferred over buoy only analysis.

Swell heights measured from the NOAA buoys are compared with those derived from the ERA5 data at the grid point nearest the buoy locations. The distances between the buoys and ERA5 grid points are 63 and 60 km for buoys 41040 and 41044 respectively. Statistical comparisons are made between datasets to assess the efficacy of the gridded product to represent in situ observations.

2.4. Characterizing and Identifying Swells

The 90th percentile of swell height is computed for each grid cell in the eastern Caribbean study area and compared to a 2.2 m threshold value. Grid cells where the 90th percentile is less than 2.2 m are masked from further analysis (Figure 2) due to the clear reduction in swell height in the Caribbean Sea from the islands. Mask location calculated from the 90th percentile of swell height versus the mean swell height does not show any signs of meaningful differences in spatial pattern.

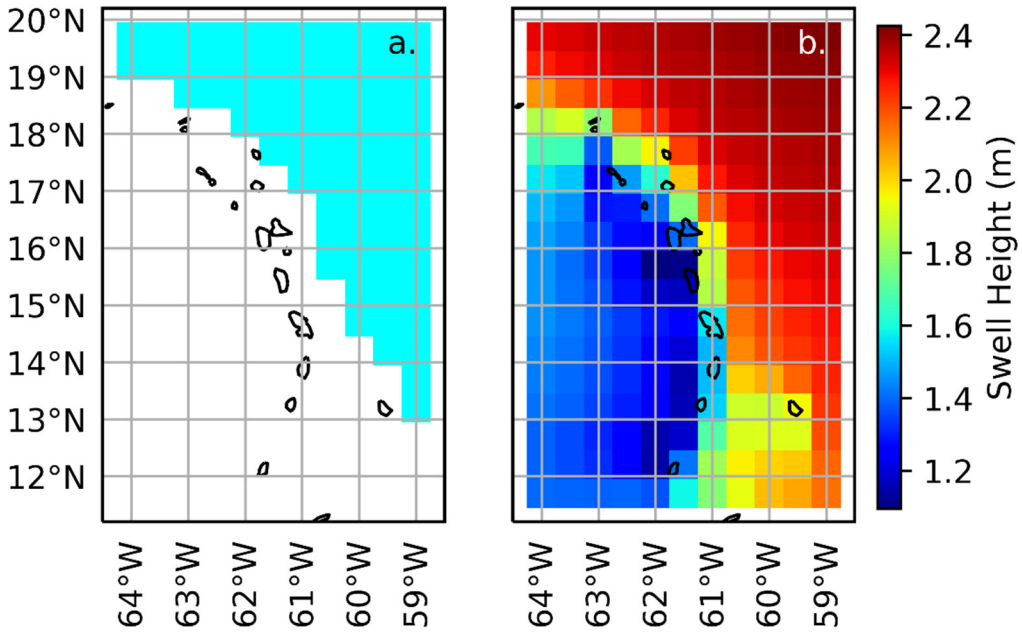

Figure 2. (**a**). Masked (white) and selected (turquoise) 0.5° × 0.5° cells for the eastern Caribbean study area. Selected cells have height ≥2.2 m in b. (**b**). 90th percentile values of swell height over study period.

Daily swell data for the eastern Caribbean are summarized by calculating spatial averages and then monthly averages from the daily spatial averages. Such summary data are also grouped by swell direction in 22.5° bins.

An empirical orthogonal function (EOF)-clustering procedure is used to identify the most recurrent patterns in the swell data, as well as north swell days and events (defined below) [20–22]. Masked grids for the eastern Caribbean swell study area of daily swell height, period, and the x and y components of direction serve as initial inputs to the EOF-clustering procedure. Prior to calculating the EOF, daily input values are standardized by subtracting the long-term gridded mean over the available 40-year period and dividing by the gridded standard deviation. Inputs are weighted by the cosine of the grid cell latitude to account for the decreasing grid cell size moving poleward [21]. Following Dawson [23], an EOF analysis is computed to reduce the redundancy in the input data and provide orthogonal inputs for the cluster analysis. Five EOF structures (spatial patterns) and their corresponding principal components (PC's; time series), which collectively explain 97.4% of the total variance in the input data and individually each explain over 1% of the variance, are retained for continued analysis (Figure S1a).

Spatial patterns of daily swell height, period, and direction are grouped using a k-means clustering analysis calculated from the five PC's [24–26]. The k-means method iteratively repartitions days into clusters to minimize the sum of variances within the clusters. The analysis is executed ten times with a predetermined number of clusters ranging from 1–10. Each of the ten individual analyses is initialized 50 times with different randomly generated cluster centers. The maximum number of iterations to minimize the sum of variances for each initialization is set to 500. This maximum is never reached as the algorithm converged on a solution well prior to this maximum. The initialization with the smallest sum of squared error (SSE) when comparing the Euclidian distance between cluster centers and cluster members is chosen. The three clusters used for this analysis are identified by the curve "elbow", which highlights the optimum cluster number where a decrease in SSE tends to plateau as the number of clusters increases (Figure S1b). Two and four cluster results are also examined and found to be biased: two clusters did not account for one of the three major swell patterns and four clusters unnecessarily subdivided one of them.

Cluster composite maps of swell height, period, and direction are created by averaging data from all the member days for each cluster. Monthly counts of cluster occurrence are calculated from the time series of daily cluster membership. Daily spatial averages of swell height, period, and direction are calculated for the cluster representing north swells. North swell days, defined as days belonging to the north swell cluster, are aggregated into north swell events by grouping consecutive north swell days. To separate back-to-back north swell events without non-north swell days in between, the second event is determined to begin when the spatially averaged swell height increased after falling at the end of the first event. Finally, the parameters of a generalized extreme value (GEV) distribution [15,27,28] are fit to the time series of the annual maximum spatially averaged swell height to assign a probability of occurrence to each north swell day. North swell events are assigned the probability associated with the lowest probability (i.e., highest height) day of the event.

2.5. Atmosphere and Swell Composites and Anomalies

Atmosphere and swell composites are created for the entire study area to examine the broader geographic conditions and forcing mechanisms associated with each cluster. Composites of sea level pressure, wind speed and direction, and swell height, period and direction are calculated for the full study area by averaging the gridded data for the days in each of the three clusters. Additionally, days within the north swell cluster are also composited in three classes according to their swell height probability (Low (Lo): <0.25, Medium (Md): 0.25–0.75, and High (Hi): >0.75). Composite anomalies are mapped based on differences between the previously described composites and the gridded long-term NDJFMA mean of each variable. Composites and anomalies are mapped for the four days prior to the day belonging to a specific cluster or a specific probability category of the north swell cluster to show the evolution of the atmospheric patterns leading to the swell generation. Swell days prior to November 4 are not included in this analysis because the preceding days are not available in the considered dataset.

2.6. Identifying Storms and Their Relationship to the North Swell

A methodology is developed to identify transient centers of low surface pressure offshore of the Atlantic coast of North America, which are hypothesized to generate most north swells that propagate into the eastern Caribbean. Numerous examples exist for identifying storm tracks in reanalysis data [29–36]. The present study most closely follows Hirsch et al. [30]. For each day, the minimum sea level pressure grid cell location is identified as well as the 40 cells that form the edge of an $11^\circ \times 11^\circ$ square centered on the minimum surface pressure location. The minimum surface pressure center is determined to be a closed low if at least 80% of the edge cells of the $11^\circ \times 11^\circ$ square are over 4 hPa higher than the minimum pressure. A closed low is a standard criterion in automated storm identification [30]. Numerous combinations of geographical domains to examine storms,

distances away from the minimum pressure, and pressure differences are all examined and lead to similar results. The storm identification criteria are confirmed by visual inspection of daily sea level pressure animations.

Consecutive days with closed low pressure systems are identified as belonging to the same storm event if the low-pressure system on each consecutive day remains east of the previous day's location. Different thresholds of eastward displacement on consecutive days are tested and do not have meaningful impacts on the results. One-day storms are removed from the list as the overwhelming majority are assumed to be too small and short-lived to be consequential for swell generation. The following parameters are recorded for each storm system: start and end dates, duration, daily minimum pressure, and daily latitude and longitude. A probability of occurrence of each storm's lifetime minimum surface pressure value was assigned from a GEV distribution based on the inverted annual minimum pressure time-series. The annual minimum time series is inverted by subtracting from a constant value of 2000 because GEV distributions are typically based on maxima in the data [28].

Each swell event is matched with a storm event if the swell event start date was greater or equal to the storm event start date and less than or equal to 2 days after the storm event end date. The two-day lag is based on the approximate time for swells to reach the eastern Caribbean based on the composite analysis described previously. Swells with a probability below 0.75 (59 highest-height swell events) and their corresponding storms are manually inspected to ensure that swells are properly matched to storms. Four one-day storms that produced swells are added back to the dataset. Composites and anomalies of ten medium probability swell events and one low probability swell event, all with no associated storm system, are mapped following the previously discussed technique (See Table S1 for the list of these events).

Storm tracks are mapped based on the following categories: storms that produced north swells (in the eastern Caribbean) with swell height probabilities <0.25, 0.25–0.75, and >0.75, and storms that did not produce north swells (as defined by membership in the north swell cluster) with pressure probabilities <0.25, 0.25–0.75, and >0.75. The average latitude and longitude are determined for the track start, end, overall track average, and location of minimum pressure for each of these six storm categories.

3. Results

3.1. ERA5 Versus Buoy Data

Overall, ERA5 underestimates buoy observations of swell height for both buoy locations (Figure 3). This is consistent with previous studies [15,37,38]. Significant ($p < 0.01$) positive correlations exist for both locations between ERA5 and the buoy data (r = +0.76 and +0.87 for buoys 41040 and 41044, respectively). The root mean squared error between the observations and ERA5 is larger for buoy location 41040 (RMSE = 0.45 m) compared to buoy location 41044 (RMSE = 0.34 m). Some errors may exist due to an apparent low-end bias with ERA5 (Figure 4). A larger frequency count of swell heights between 1.3–2.0 m is noticeable for ERA5 for both buoy locations relative to the buoy observation, whereas a lower count of heights greater than 2.1 m is also noticed. This bias is more pronounced for buoy 41040 compared to buoy 41044. Explaining the larger error for buoy 41040 is beyond the scope of this work, but one hypothesis suggests that the proximity to the prevailing northeasterly trade winds may cause local effects in the 41040 record if the swell separation frequencies differ between the buoy observations and ERA5.

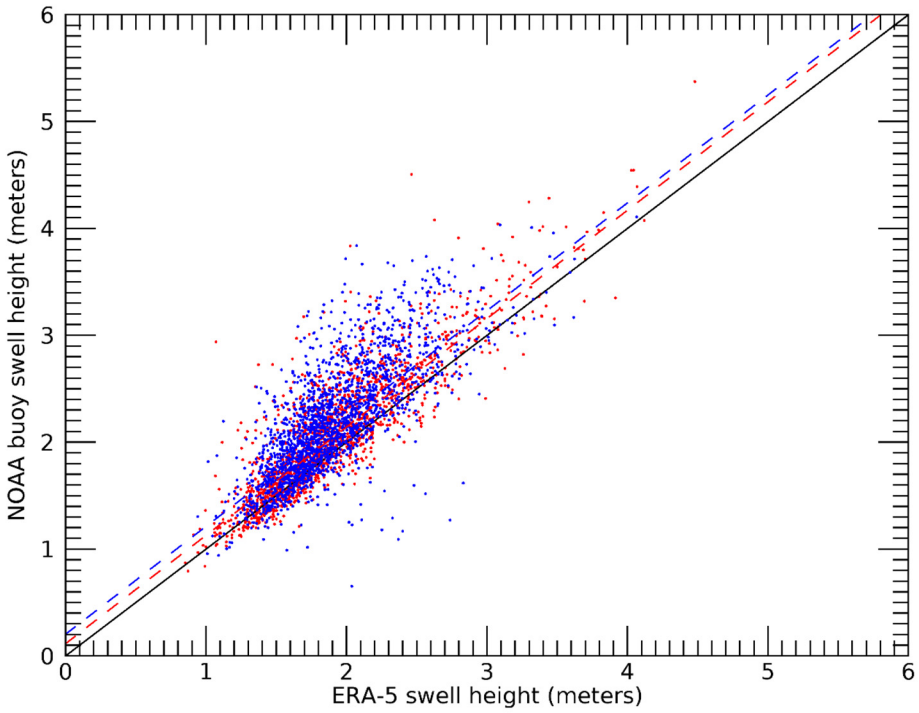

Figure 3. Distribution of daily swell height from ERA5 gridded estimates and NOAA buoy observations from the NOAA buoy 41040 (red) and 41044 (blue) locations. Dashed lines are best fit lines for respective locations and solid black line is the 1:1 line.

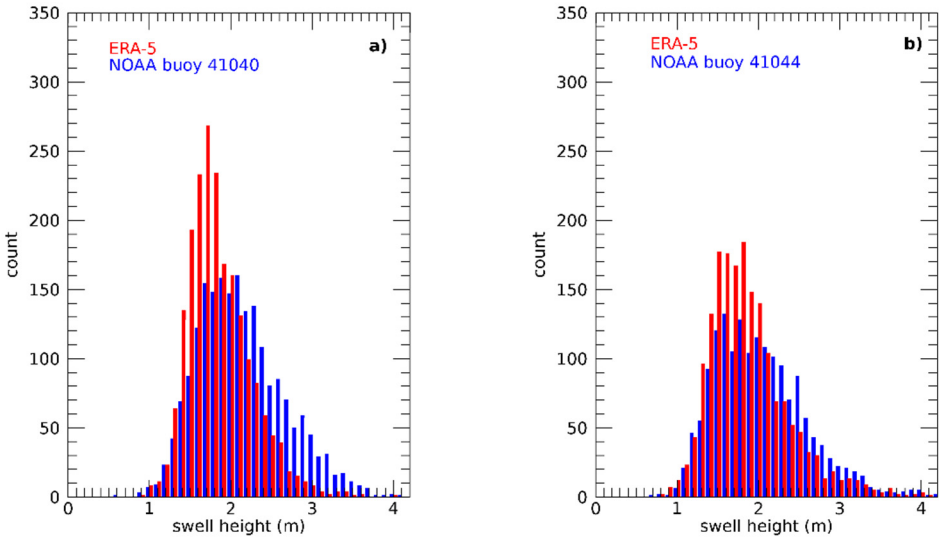

Figure 4. Count of daily swell height for ERA5 estimates and NOAA buoys (**a**) 41040 and (**b**) 41044.

The seasonal cycle between the buoy observations and ERA5 show similar patterns with larger swell heights measured between December to February and a peak median swell height in January for buoy 41040 and December for buoy 41044 (Figure 5). ERA 5 reanalysis data are deemed acceptable for the remainder of the analysis based on these comparisons.

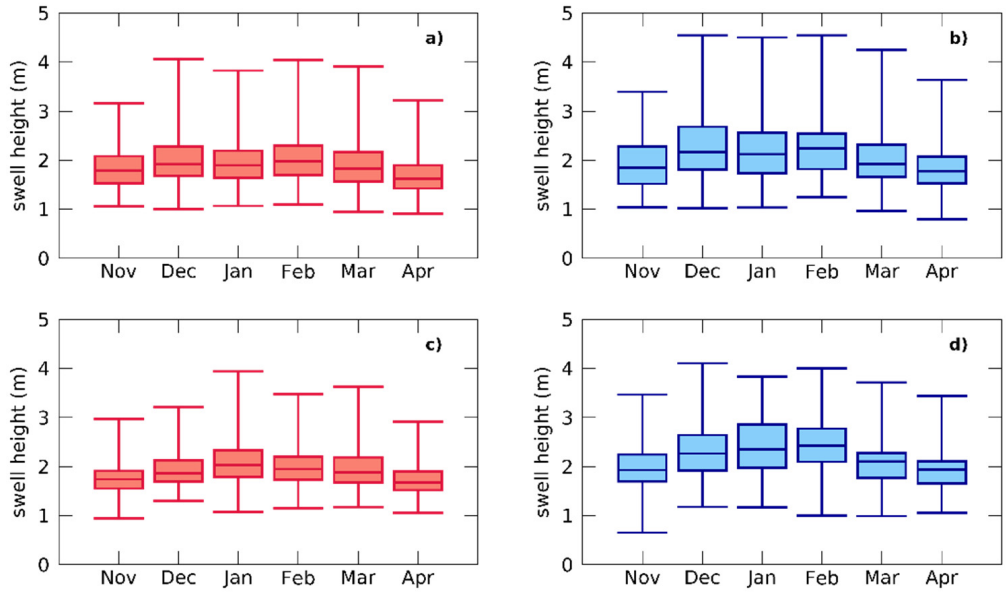

Figure 5. Average monthly swell heights for (**a**) ERA5 at buoy 41044, (**b**) buoy 41044, (**c**) ERA5 at buoy 41040, and (**d**) buoy 41040. Box plots are defined by minimum, lower quartile, median, upper quartile, and maximum.

3.2. Summary of Eastern Caribbean Swell Conditions

99.8% of daily spatially averaged swell directions have values between the 22.5° bins labeled 337.5° (NNW) and 90.0° (E) and no values between the bins labeled 135° (SE) and 247.5° (WSW) (Figure 6). There are only 11 days total (0.2% of all days; occurrences listed in the Figure 6 caption) where swell direction is from 112.5° (ESE) or from 270° (W)–315° (NW). Swell direction was most frequent (36.6%) from 67.5° (ENE) (Table 1). This is true for all individual months, except November, where swell frequency was higher from 45° (NE) (Figure 6). Purely northerly swells (0°) are most frequent in March (9.4% of all March days), February (8.3% of all February days), and January (7.4% of all January days). Maximum swell height is greatest on average from a direction of 0° (N) with highest heights occurring in March, while maximum period is largest on average from a direction of 22.5° (NNE) with the longest periods occurring in March from 0° (N). Average values are also calculated (not shown) in addition to the maximum swell height and period values shown in Figure 6. The monthly and directional patterns of average data are very similar to the patterns of the maximum data. Maximum swell height and period are on average ~1.6 and ~1.3 times larger than average swell height and period, respectively.

3.3. Characterizing Swell Conditions and Identifying North Swells

The clusters from the EOF-cluster analyses are named north (N), northeast (NE), and east (E) based on the closest cardinal or ordinal direction associated with the prevailing composite swell direction (Figure 7) and represent 1123 (16%), 2631 (36%), and 3496 (48%) days respectively. The N swell cluster is characterized by higher swell heights (2.0–2.5 m) and longer swell periods (10.2–10.6 s) compared to the NE (1.7–1.9 m, 8.8–9.0 s) and E (1.5–1.7 m, 8.1–8.2 s) clusters.

Days in the N swell cluster, which is the focus of the present study, are most frequent from December through March with the highest counts in December (243) and March (227) (Figure 8a). Swell direction during N swell days is most northerly in February (11.4°), March (14.5°), and January (16.4°) (Figure 8b). These are the same months with the lowest swell probabilities (Figure 8c). Swell heights are highest on average from December through February (2.4 m) and only slightly lower in March and November (2.3 m) (Figure 8d). Swell periods are smallest in November and January (10.4 s) and longest in December and March (10.5 s) (Figure 8e). Figure 8 differs from Figure 6 in that Figure 6 averages days based on

the daily spatial average of swell direction only, while Figure 8 averages days based on membership in the N swell cluster, which accounts for swell direction, height, and period. North swell events with a probability <0.75 are listed in Table S1.

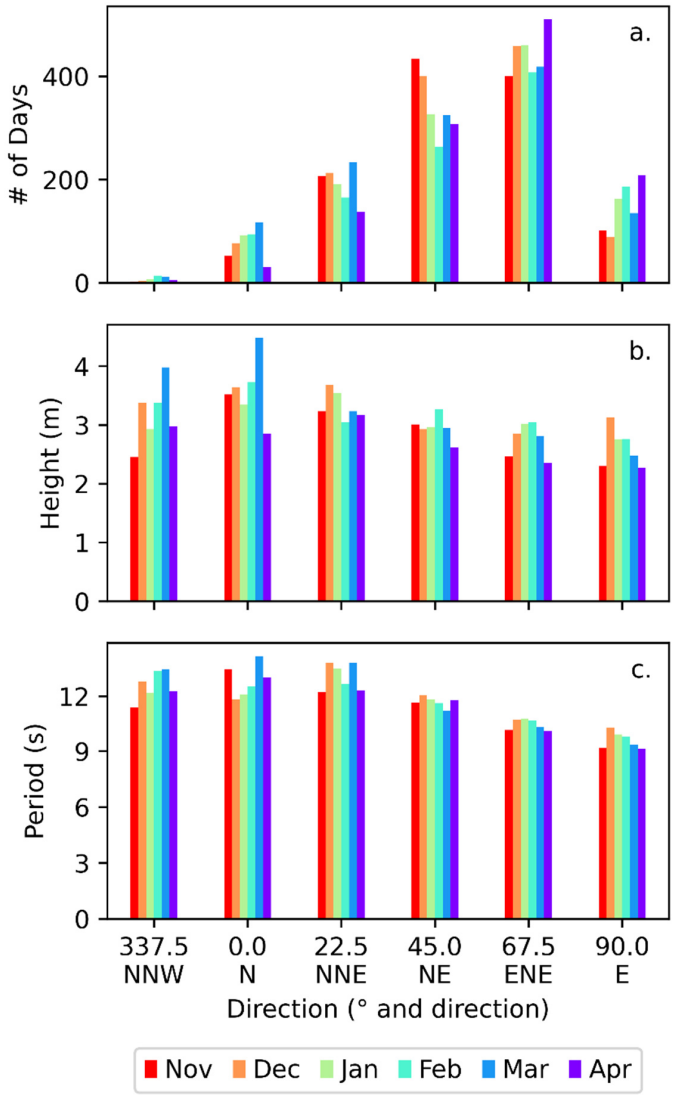

Figure 6. (**a**) Number of days by month over the 40-year study period for swells from different directions. Daily maximum swell (**b**) height and (**c**) period, spatially averaged over the eastern Caribbean study area by month and swell direction. Direction labels represent the center point of each 22.5° bin. Directions from 112.5° to 315.0° are not shown and have swell counts of zero except for the following month/direction pairs: Nov/112.5° = 1, Nov/270.0° = 1, Nov/292.5° = 2, Jan/112.5° = 1, Jan/315.0° = 1, Feb/112.5° = 1, Mar/112.5° = 1, and Apr/112.5° = 3.

Table 1. Total number and percentage of days, and average maximum swell height and period for those days, binned by direction based on the monthly data shown in Figure 6.

Direction (°)	# of Days	% of Days	Max Height (m)	Max Period (s)
337.5	44	0.6	3.2	12.6
0.0	462	6.4	3.6	12.8
22.5	1145	15.8	3.3	13.0
45.0	2054	28.4	3.0	11.7
67.5	2653	36.6	2.8	10.5
90.0	881	12.2	2.6	9.6

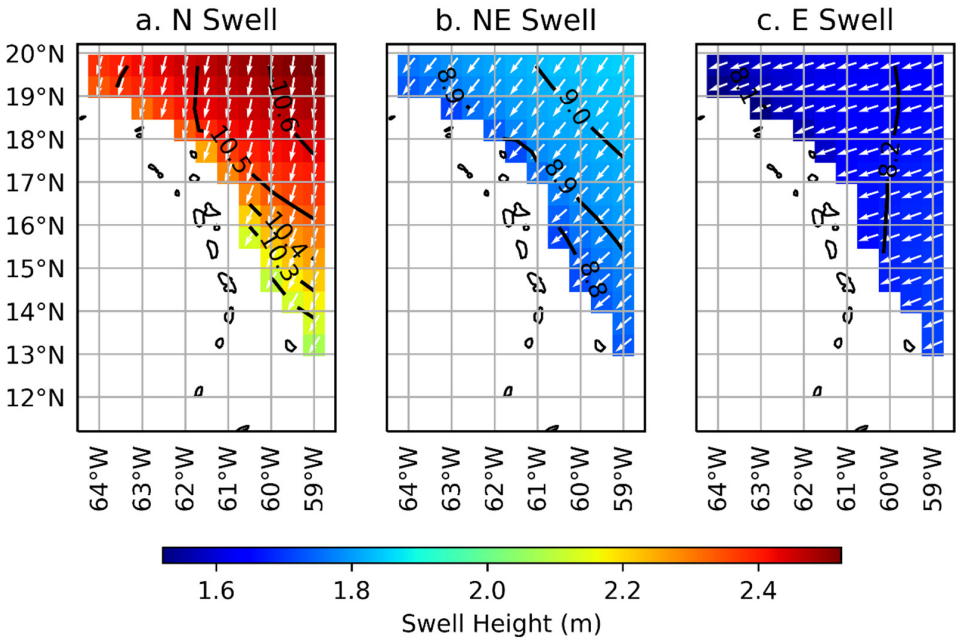

Figure 7. Composite averages of swell height (color), period (contours; units = seconds), and direction (arrows) for the (**a**) north, (**b**) northeast, and (**c**) east swell clusters.

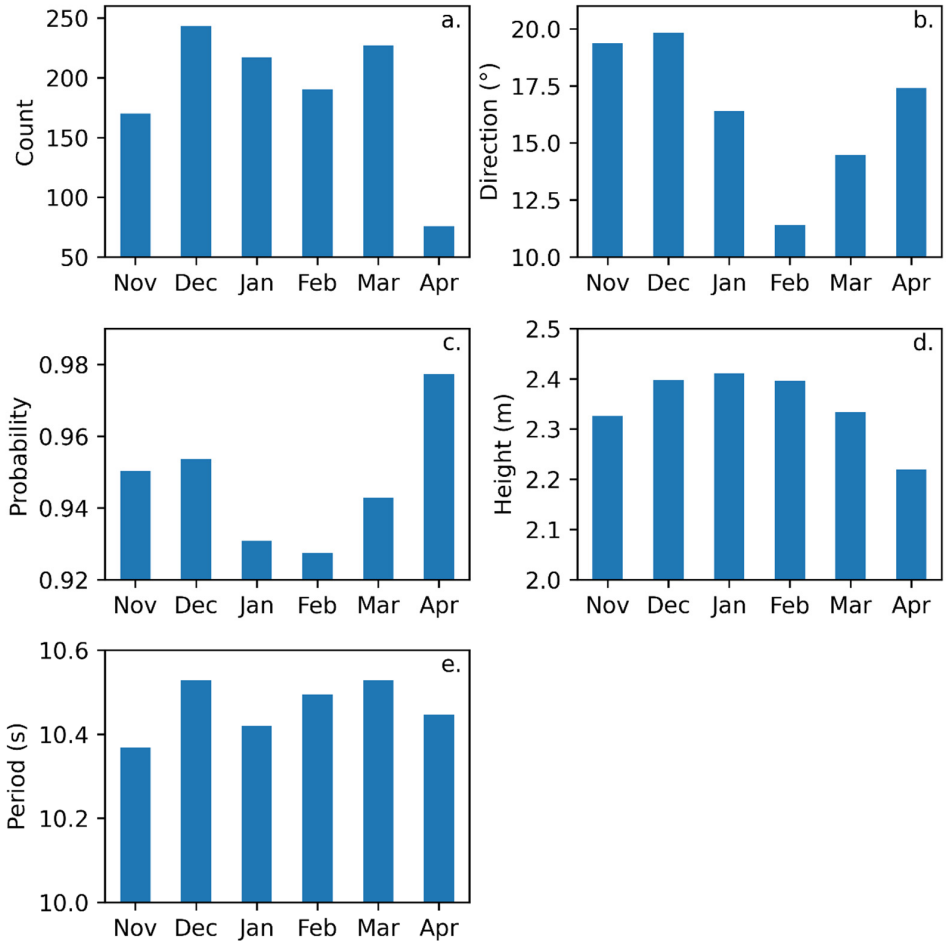

Figure 8. (**a**). Monthly count of north swell cluster (Figure 7a) days for the study period. Daily spatially averaged data for the eastern Caribbean for north swell cluster days, averaged by month, of swell (**b**). direction, (**c**). probability, (**d**). height, and (**e**). period.

3.4. Atmosphere and Swell Composites and Anomalies

The average winter sea level pressure pattern is characterized by a subtropical high-pressure system in the eastern North Atlantic Ocean around 35° N and an Icelandic low pressure off the southeast coast of Greenland (Figure 9a). Surface wind speeds are greatest and dominantly westerly in the northern part of the study area where the horizontal pressure gradient is tighter, least in the latitudinal belt associated with the subtropical high-pressure system, and slightly higher and easterly to northeasterly in the tropics, including the eastern Caribbean. Average wind direction in the tropics and eastern Caribbean is easterly to northeasterly. Correspondingly, values of swell height and period are highest in the northern part of the study region which broadly corresponds to the area where wind speeds are fastest and thus enable the outbound propagation of large swells (Figure 9b). Swell direction on the Atlantic side of the eastern Caribbean is northeasterly.

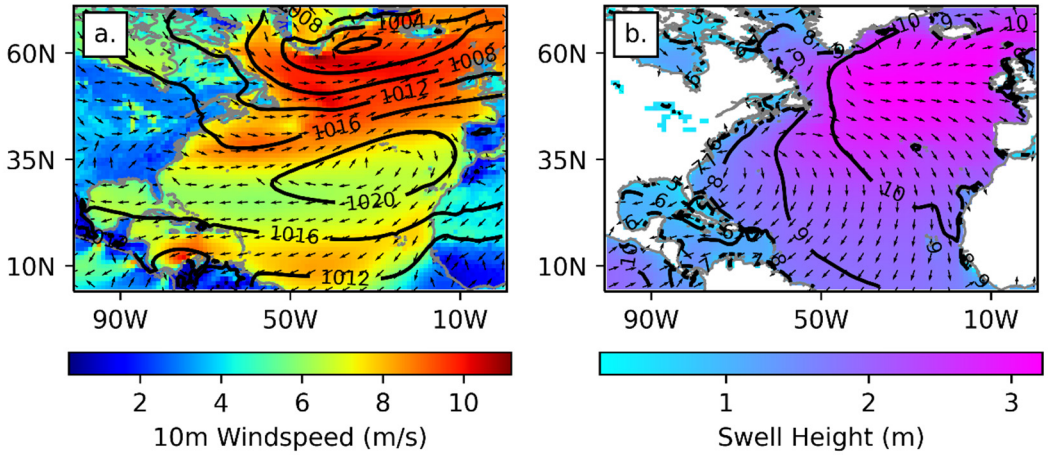

Figure 9. (**a**). NDJFMA seasonal average sea level pressure (contours, hPa), surface wind speed (shading), and direction (arrows). (**b**). NDJFMA seasonal average swell period (contours, s), height (shading), and direction (arrows). Both maps represent all days in the study period.

Negative surface pressure and positive wind speed anomalies for the N swell cluster (Figure 10, row 1), beginning on day −4 and peaking on days −3 and −2, indicate the presence of a low-pressure system off the east coast of North America. The strongest winds are northerly to northwesterly and are located on the system's southwestern flank. These winds generate positive swell height and period anomalies that become largest from day −2 to day 0 and propagate southward across the basin (Figure 10, row 2). Swell anomalies are largest on day −1 before the Caribbean Islands presumably begin to dampen the swell on day 0. The low-pressure system begins to weaken on day −1 as it propagates eastward toward Europe.

The anomalies for the NE swell cluster (Figure 10, rows 3–4) are the closest ones to zero among the three clusters, indicating conditions most like the NDJFMA average presented in Figure 9. A belt of slightly slower wind speeds exists in the tropics and slightly higher wind speeds exist in the subtropics, with weakly positive swell height anomalies in the basin western half.

Sea level pressure anomalies for the E swell cluster in the western Atlantic around 35° N are higher in the days leading up to day 0 (Figure 10, row 5), indicating a westward shift in the average location of the Atlantic high-pressure system in Figure 9. Correspondingly, wind speeds in the tropical North Atlantic are faster. Of the three swell clusters, E swells on average are characterized by the lowest heights and shortest periods (Figure 7). This can be seen in the negative height anomalies that become greatest from day −2 to day 0 in the southern part of the basin (Figure 10, row 6).

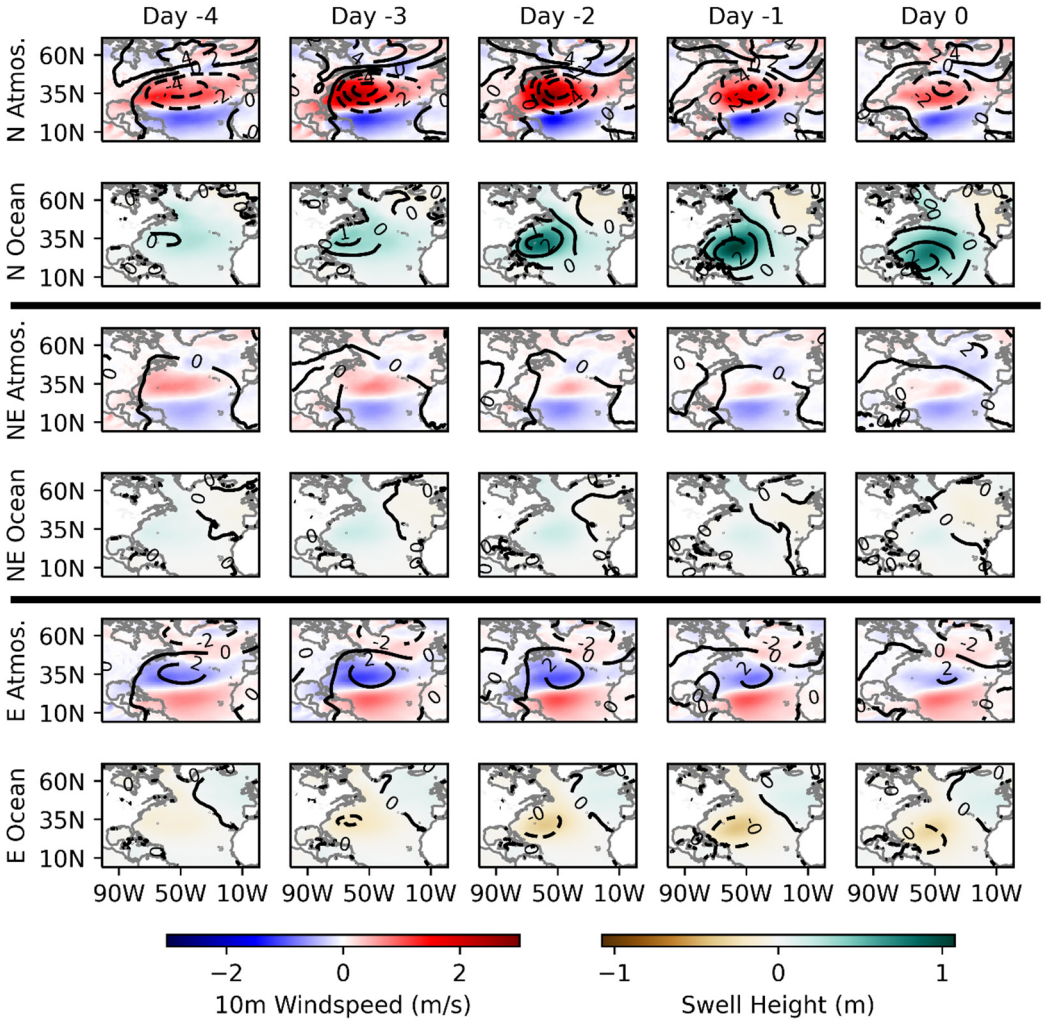

Figure 10. Atmosphere (rows 1, 3, and 5) and ocean swell (rows 2, 4, and 6) anomaly composites for the north cluster (rows 1–2; 1092 days composited), northeast cluster (rows 3–4; 2517 days composited), and east cluster (rows 5–6; 3401 days composited). Anomalies are composite average differences from the climatological mean atmosphere and ocean swell maps presented in Figure 9. Shading is the surface wind speed or ocean swell height anomaly. Contours are the sea level pressure (hPa) or ocean swell period (s) anomaly. Anomalies of surface wind and swell directions are not shown. Day 0 is the day that was classified as belonging to one of the three clusters. Days −1 to −4 represent the 4 days prior to Day 0.

The atmosphere and swell anomalies for N swell cluster days with different probabilities (Figure 11) show similar patterns across the three probability categories. Anomaly absolute values are largest for the low probability swell days (Figure 11, rows 1–2) and smallest for the high probability days (Figure 11, rows 5–6). For all three north swell probability categories, negative sea level pressure and positive wind speed anomalies off the east coast of North America, intensifying on day −3, indicate the presence of a storm system in this area with faster northwesterly winds on the system's southwest side (Figure S2) and result in positive swell height and period anomalies from day −2 to day 0. The lowest sea level pressure, highest wind speed, highest swell height, and highest period anomalies are −17.4 hPa, 7.3 m/s, 2.7 m, and 4.9 s for low probability days (rows 1–2) and −7.4 hPa, 2.8 m/s, 1.0 m, and 1.8 s for high probability days (rows 5–6), respectively.

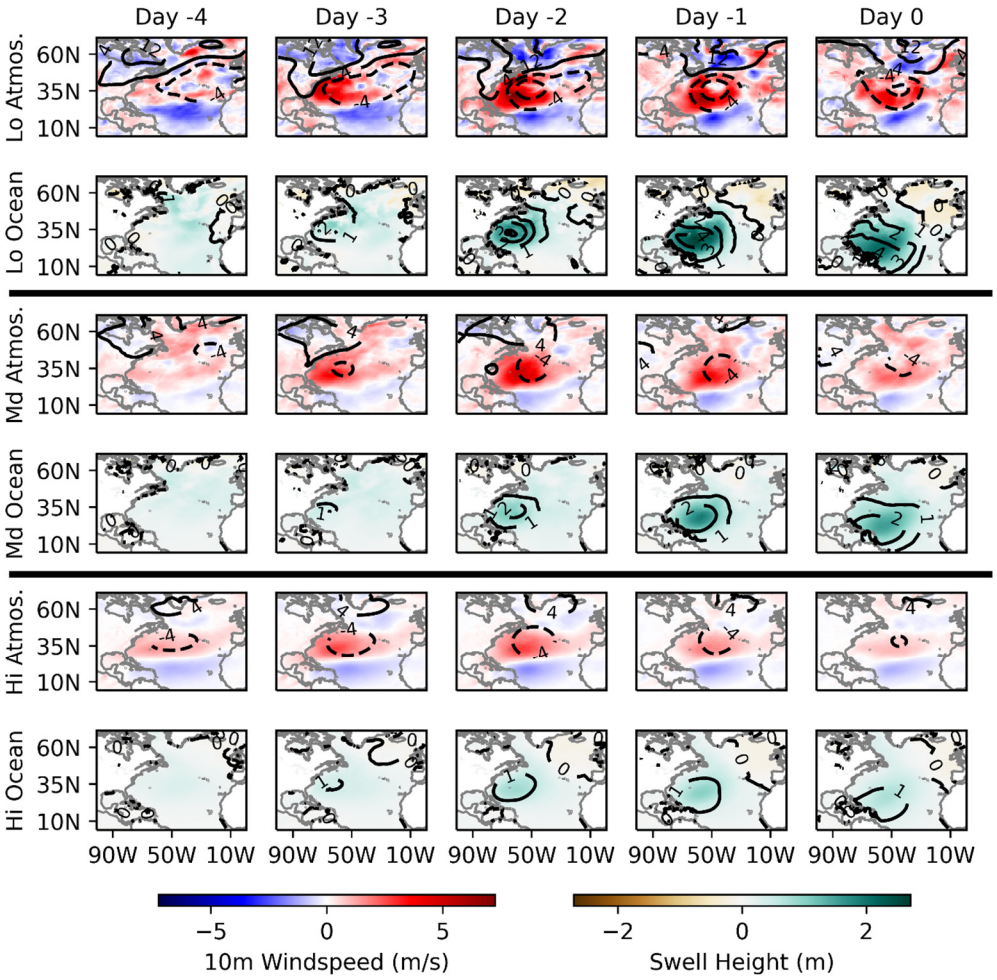

Figure 11. Same as Figure 10 except anomaly composites for low probability north swell events (Lo; rows 1–2; 12 days composited), medium probability north swell events (Md; rows 3–4; 75 days composited), and high probability north swell events (Hi; rows 5–6; 1036 days composited). Probabilities are defined as: Lo < 0.25, 0.25 ≤ Md ≤ 0.75, Hi > 0.75. Day 0 is the day that was classified as belonging to one of the three swell probability groups.

3.5. Identification of Storms and Their Relationship to North Swells

Low probability north swell events in the eastern Caribbean (Table S1), on average, are associated with storms that have a more southern and eastern average location and a more zonal trajectory (Figures 12a and 13). Storms that produce moderate (Table S1) and high probability north swell events have a more southwest-to-northeast trajectory, with the storms that produce high probability swell events being located further northwest (Figures 12b,c and 13). Compared to the aforementioned three storm categories, storms that do not produce north swell events in the eastern Caribbean are located further north on average (Figures 12d–f and 13). Among these, the high probability storms that do not produce swells are, on average, located south and well west of the moderate and low probability storms that do not produce swells.

Maximum spatially averaged swell height in the eastern Caribbean for north swell events is highly correlated with swell period (r = 0.71, $p < 0.01$) (Table 2). Swell height is also significantly correlated with the latitude of the storm minimum pressure location but with weaker, negative correlation (r = −0.19, $p < 0.01$). The correlation between swell height and the longitude of the storm minimum pressure location (r = 0.13, $p < 0.02$) and the daily average longitudinal distance traveled (r = −0.13, $p < 0.02$) are also significant. Storms located further south and east that move more slowly in the longitudinal direction correlate with north swell events with higher heights, consistent with the previous analysis

(Figures 12 and 13). North swell direction, storm minimum pressure, and average latitudinal distance traveled are not significantly correlated with north swell height, indicating that storm location and speed are more important than storm pressure in determining north swell height.

3.6. Non-Storm Driven Swells

11 of the 59 north swell events with a probability <0.75 do not have storms associated with them (Table S1). Ten of these events are categorized as moderate probability events (range = 0.36–0.68) and one event is categorized as low probability (0.11). Positive sea level pressure anomalies for the moderate swell events exist on days −3 to −1 in the western Atlantic region of the study area, indicating that the North Atlantic high-pressure system in Figure 9 has shifted well west of its average NDJFMA location (Figure 14, row 1). Correspondingly, positive wind speed anomalies peak on days −3 to −1 south of the high-pressure anomalies and have a northerly direction (Figure S3, row 1). The resulting positive swell height and period anomalies occur in the eastern Caribbean on day −1 and day 0.

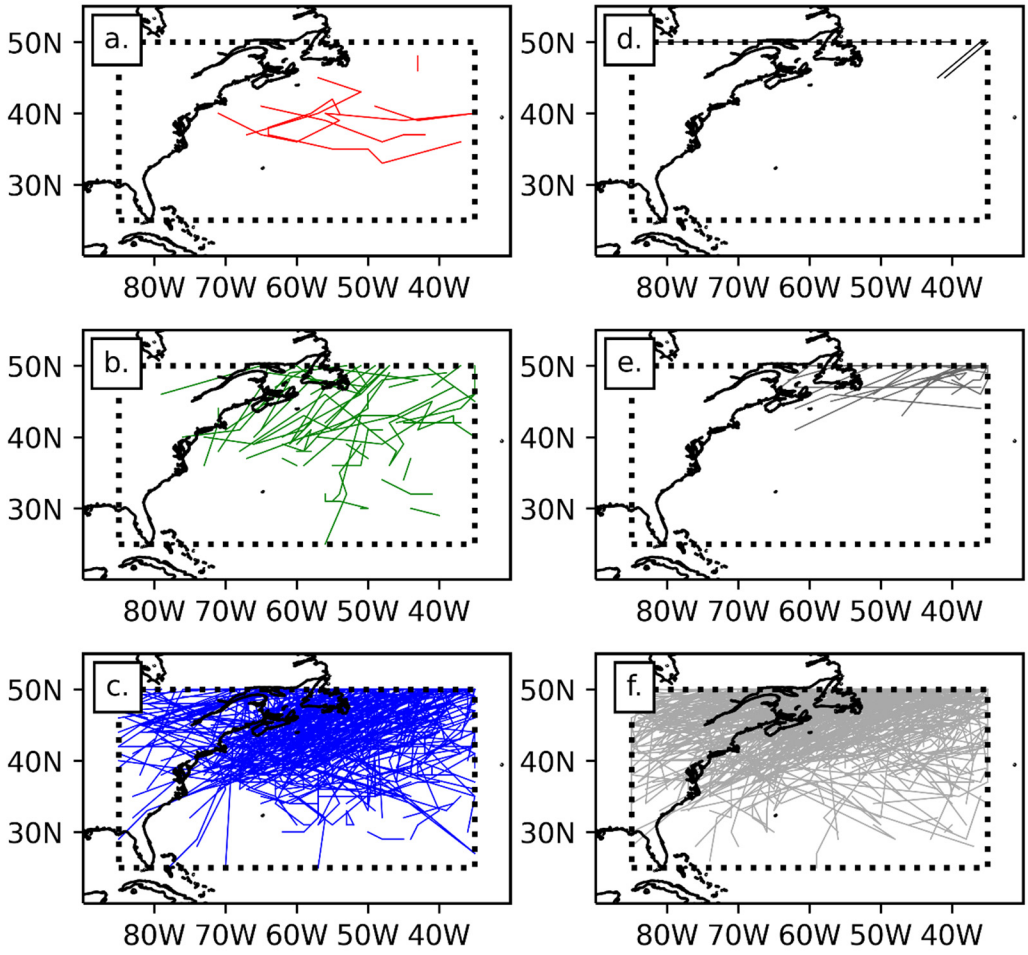

Figure 12. (**a**–**c**) Storm tracks for low pressure systems that generated north swells in the eastern Caribbean study area with swell probabilities (**a**) <0.25, (**b**) 0.25–0.75, and (**c**) >0.75. (**d**–**f**) Storm tracks for low pressure systems that did not generate north swells in the eastern Caribbean study area with storm probabilities (**d**) <0.25, (**e**) 0.25–0.75, and (**f**) >0.75. The dotted rectangle is the area used to constrain the storm identification algorithm.

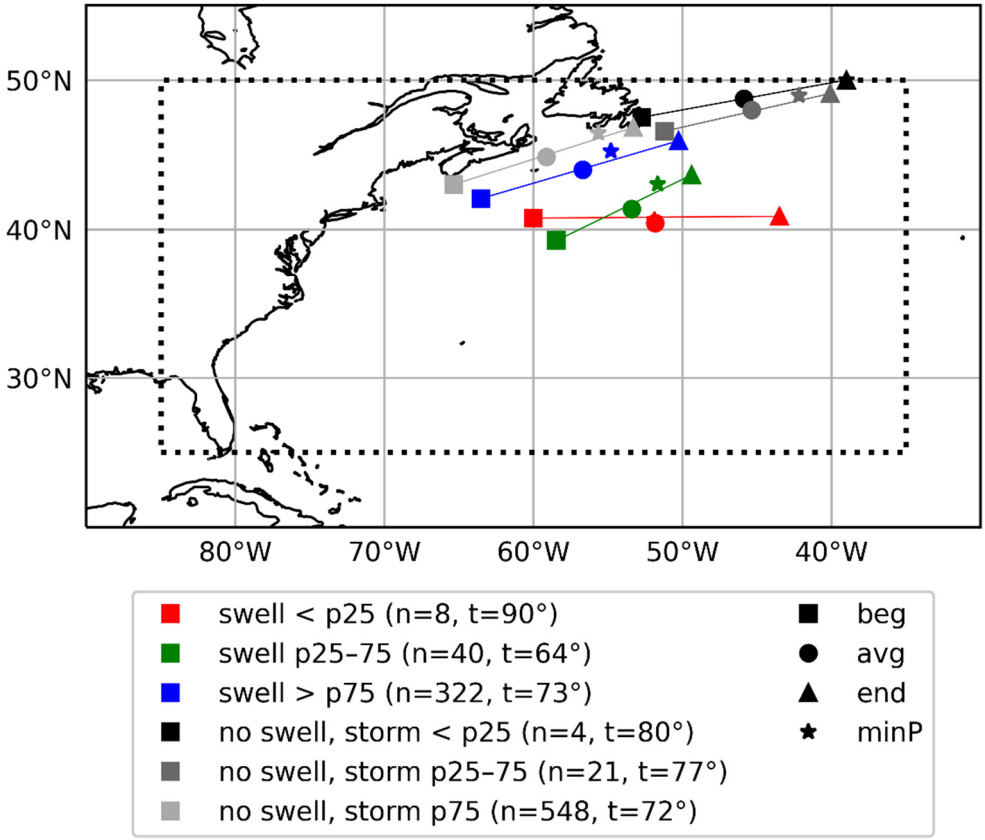

Figure 13. Average storm tracks based on the individual tracks shown in Figure 12. The dotted rectangle is the area used to constrain the storm identification algorithm. Red, green, and blue tracks are for storms that generated swells of different probabilities in the eastern Caribbean study area. Gray-scale tracks are for storms of different probabilities that did not generate north swells in the eastern Caribbean study area. p25, p25–75, and p75 are swell or storm probabilities <0.25, 0.25–0.75, and >0.75, respectively. n represents the number of storms that were used to create the average track. t is the direction of the average track, where 0° represents south to north and increases clockwise. beg and end represent the average locations on the first and last days that the storm was identified by the algorithm. avg is the average location for all days of the averaged storm tracks and minP is the average location where the storm sea level pressure was lowest.

Table 2. Pearson correlation coefficients r and corresponding *p*-values for relationships between spatially averaged maximum swell heights for north swell events in the eastern Caribbean study area on the one hand, and the three swell (period, zonal, and meridional components) or storm (minimum pressure, latitude and longitude of minimum pressure, and average daily distance traveled) variables on the other hand.

Variable	r	*p*
Swell Period	0.712	0.000
Swell Zonal Component	0.010	0.830
Swell Meridional Component	0.030	0.515
Storm Minimum Pressure	−0.019	0.717
Storm Minimum Pressure Latitude	−0.187	0.000
Storm Minimum Pressure Longitude	0.125	0.016
Storm Daily Average Latitudinal Distance	0.022	0.679
Storm Daily Average Longitudinal Distance	−0.132	0.011

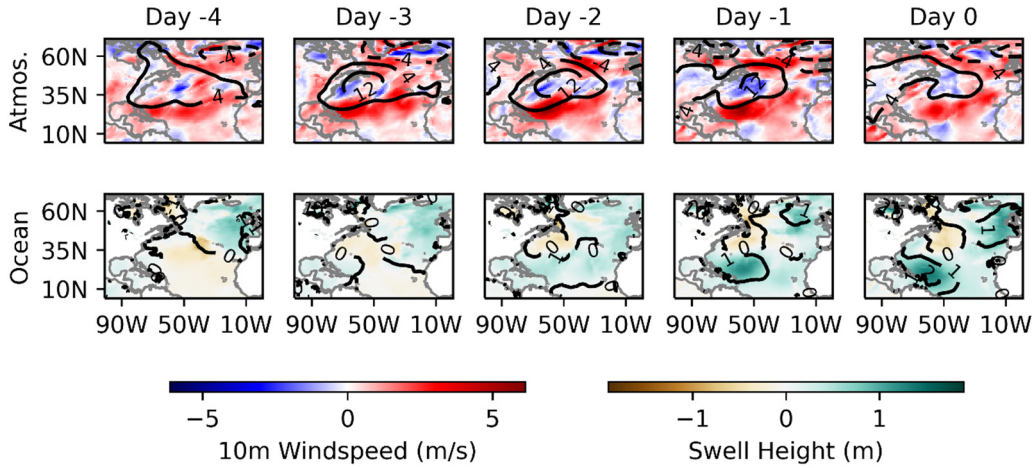

Figure 14. Same as Figure 10 except anomaly composites for high pressure induced, medium probability north swell events (10 days composited per map). Day 0 is the day that was classified as a north swell day.

The single low probability north swell event without an associated storm represents a hybrid of the storm-induced and high-pressure-induced north swell events. Sea level pressure anomalies on day −2 are positive in the eastern and western portions of the study area around 35° N (Figure 15, row 1). Negative anomalies exist in between the positive anomalies, indicating the presence of two distinct high-pressure systems on the eastern and western sides of the study area, and a low-pressure area "sandwiched" in between that represents a frontal boundary associated with the low-pressure system to the north (Figure S4). The resulting positive wind anomalies are associated with the zonal pressure gradient between the "sandwiched" low and the western high that produces northerly winds on days −2 to −1 and positive swell height and period anomalies on days −1 and 0 (Figure 15, row 2).

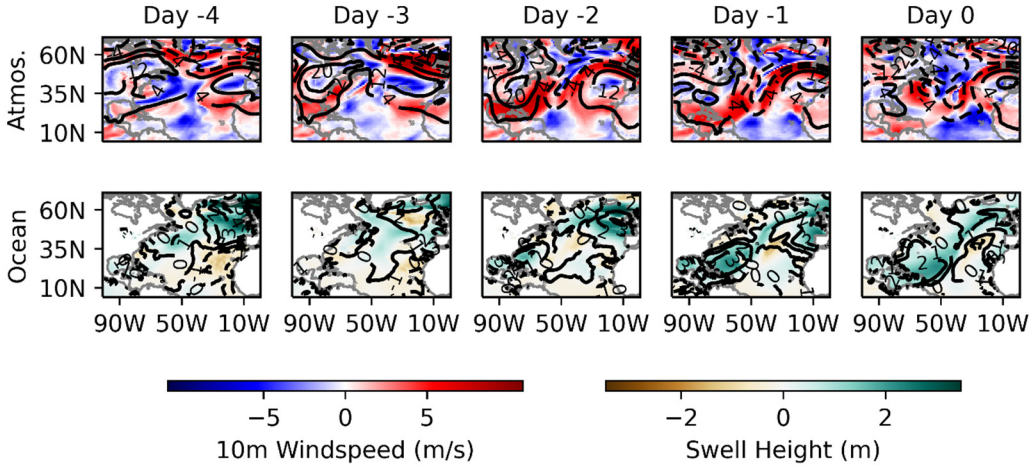

Figure 15. Same as Figure 10 except anomaly for the single high pressure induced, low probability north swell event (day 0 = 12/22/1991). Day 0 is the day that was classified as a north swell day.

4. Discussion

This study makes use of ERA5 reanalysis data to examine north swell events in the eastern Caribbean. Compared with buoy observations, ERA5 underestimates swell height; an observation consistent with previous studies [15,37,38]. ERA5's higher spatial and temporal coverage, however, make it an acceptable dataset for this study. Underestimates of swell height may have implications when assessing the magnitude of coastal hazards.

Jury [7] notes that near Puerto Rico, northerly (315°–45°) swells occur 29% of the time on an annual basis with a mean height and period of 2 m and 8 s respectively. For the present study in the eastern Caribbean, the north swell cluster occurs 16% of the time during the NDJFMA period with monthly average swell height and period ranges of 2.2–2.4 m and 10.4–10.5 s respectively. Additionally, a more southeasterly and zonal storm track is associated with larger north swell heights in the eastern Caribbean.

The highest-height north swell event for both the present study and Jury [7] is associated with a storm on 16–20 March 2008. Jury [7] shows a blocking high sea level pressure system near Greenland slows the storm movement and allows more persistent northerly winds to generate the swell that ultimately impacts Puerto Rico. Jury [7] also notes that a similar blocking high exists for the next five highest events in the study. A similar sea level pressure pattern is seen in the low probability north swell composite anomalies (Figure 11, row 1), where the negative pressure anomalies around 35° N associated with storms immediately transition to positive pressure anomalies to the north in a location similar to Jury [7]. Pressure anomalies with a similar pattern but smaller absolute values exist for both the moderate and high probability north swell events (Figure 11, rows 3 and 5). The blocking high prolongs the duration of northerly winds generated from a region favorable for north swell propagation toward Puerto Rico and the eastern Caribbean. After reaching Puerto Rico, north swells take approximately 1 day longer to propagate to the eastern Caribbean.

In the North Atlantic, the annual cycle and low-frequency modes of both large-scale and synoptic atmospheric patterns induce strong seasonality and interannual variability of wave climate. On interannual time scales, Woolf et al. [3] have shown the strong relation between ocean waves, particularly in the northeastern part of the sub-basin, and the North Atlantic Oscillation (NAO), which is the dominant mode of atmospheric variability over the sub-basin and is associated with the pressure difference between the Azores high and the Icelandic low [39] (Figure 9a). Morales-Marquez et al. [40] further demonstrate that the NAO is a major driver of the interannual variability of wintertime extreme wave heights in this region. Future work in the eastern Caribbean should examine the relationship between north swells and the NAO. The phase and intensity of the NAO could possibly influence the storm speed and track location and therefore the generation and propagation of north swells toward the eastern Caribbean.

Additionally, to our knowledge, this is first study to identify high sea-level pressure systems in the western North Atlantic as generating moderate probability north swells in the eastern Caribbean. As such, the relationship between these high-pressure systems and their covariability with NAO phase and strength should also be examined.

The algorithm to identify storms in this study is limited. It is possible to have multiple low-pressure systems within the study area at the same time, but the algorithm only identifies the single low associated with the minimum pressure, missing any other local minima. This is due to the computational demands required to locate all closed lows for each day. Generally, such multi-low situations persist one day before one of the lows propagates out of the study region, at which point the second low is identified. Furthermore, the minimum pressure system likely has stronger winds and is therefore more likely associated with swell generation, although storm area and track speed may be of importance as well. Finally, there are never two major low-pressure systems in the study area at the same time. Rather, whenever two systems are observed, the larger one is typically in the process of moving out of the eastern or northern edge of the study area while the smaller one is forming along the western or southern edge.

Many storms in the North Atlantic do not generate north swells in the eastern Caribbean. Conceivably, some fraction of these storms generates significant swell events in locations other than the eastern Caribbean. Boucharel et al. [5] examine this idea in the Pacific basin by assessing local versus remote atmospheric drivers of swell. A similar methodology could be applied to the Atlantic basin. At the Atlantic basin or North Atlantic sub-basin scale, it would also be possible to replicate the EOF-clustering procedure presented here. This procedure, however, would illuminate basin-scale swell patterns and

not highlight patterns that are unique to a specific region such as was done here for the eastern Caribbean. As such, future research should consider a methodology to identify unique swell climate regions for more in-depth analysis or perhaps identify all storms in the sub-basin and develop composites and anomalies of swell conditions based on different storm categories.

Finally, long-term historic trends and future projections of wave-climates in the eastern Caribbean should be investigated. Future warming projections generate decreases in significant wave heights over the North Atlantic sub-basin (e.g., [41]). Belmadani et al. [15] confirm this result but also show marked increases in extreme wave heights associated with tropical storms. Future work should make use of climate projections to drive wave models for the eastern Caribbean and other local regions.

Supplementary Materials: The following supporting information can be downloaded at: https://www.mdpi.com/article/10.3390/jmse10020183/s1, Figure S1: EOF explained variance and cluster sum of squared error; Figure S2: Composite averages for Lo, Md, and Hi probability north swells; Figure S3: Composite averages for high pressure induced Md probability north swells; Figure S4: Composite averages for low probability north swell event; Table S1: North swell events.

Author Contributions: Conceptualization, I.G., T.A. and A.B.; methodology, T.W.H., I.G., T.A. and A.B.; software, T.W.H.; validation, T.A.; formal analysis, T.W.H.; investigation, T.W.H.; resources, T.W.H.; data curation, T.W.H. and T.A.; writing—original draft preparation, T.W.H., I.G., T.A. and A.B.; writing—review and editing, T.W.H., I.G., T.A. and A.B.; visualization, T.W.H.; supervision, T.W.H.; project administration, T.W.H.; funding acquisition, T.W.H. All authors have read and agreed to the published version of the manuscript.

Funding: T. Hawkins was funded as part of a Fulbright Scholar Award (10394-BB) through the Bureau of Educational and Cultural Affairs at the United States Department of State. The Government of the United States, or any agency representing it, has not endorsed the conclusions or approved the contents of this research.

Institutional Review Board Statement: Not applicable.

Informed Consent Statement: Not applicable.

Data Availability Statement: Hersbach, H. et al., (2018) was downloaded from the Copernicus Climate Change Service (C3S) Climate Data Store. The results contain modified Copernicus Climate Change Service information 2020. Neither the European Commission nor ECMWF is responsible for any use that may be made of the Copernicus information or data it contains.

Acknowledgments: The authors thank Météo-France for its strong commitment and support of A. Belmadani.

Conflicts of Interest: The authors declare no conflict of interest.

References

1. Munk, W.H.; Miller, G.R.; Snodgrass, F.E.; Barber, N.F.; Deacon, G.E.R. Directional Recording of Swell from Distant Storms. *Philos. Trans. R. Soc. Lond. Ser. A Math. Phys. Sci.* **1963**, *255*, 505–584. [CrossRef] [PubMed]
2. Young, I.R. Seasonal Variability of the Global Ocean Wind and Wave Climate. *Int. J. Climatol.* **1999**, *19*, 931–950. [CrossRef]
3. Woolf, D.K.; Challenor, P.G.; Cotton, P.D. Variability and Predictability of the North Atlantic Wave Climate. *J. Geophys. Res. Oceans* **2002**, *107*, 9-1–9-14. [CrossRef]
4. Alves, J.-H.G.M. Numerical Modeling of Ocean Swell Contributions to the Global Wind-Wave Climate. *Ocean Model.* **2006**, *11*, 98–122. [CrossRef]
5. Boucharel, J.; Santiago, L.; Almar, R.; Kestenare, E. Coastal Wave Extremes around the Pacific and Their Remote Seasonal Connection to Climate Modes. *Climate* **2021**, *9*, 168. [CrossRef]
6. Lefèvre, J.-M. High Swell Warnings in the Caribbean Islands during March 2008. *Nat. Hazards* **2009**, *49*, 361–370. [CrossRef]
7. Jury, M.R. Characteristics and Meteorology of Atlantic Swells Reaching the Caribbean. *J. Coast. Res.* **2018**, *34*, 400–412. [CrossRef]
8. Cooper, J.A.G.; Jackson, D.W.T.; Gore, S. A Groundswell Event on the Coast of the British Virgin Islands: Spatial Variability in Morphological Impact. *J. Coast. Res.* **2013**, *65*, 696–701. [CrossRef]
9. Nurse, L.; Mclean, R.; Agard, J.; Briguglio, L.; Duvat, V.; Pelesikoti, N.; Tompkins, E. Chapter 29: Small Islands. In *Climate Change 2014: Impacts, Adaptation, and Vulnerability. Part B: Regional Aspects. Contribution of Working Group II to the Fifth Assessment Report of the Intergovernmental Panel on Climate Change*; Cambridge University Press: Cambridge, UK, 2014; p. 1654.

10. Young, I.R.; Zieger, S.; Babanin, A.V. Global Trends in Wind Speed and Wave Height. *Science* **2011**, *332*, 451–455. [CrossRef]
11. Timmermans, B.; Stone, D.; Wehner, M.; Krishnan, H. Impact of Tropical Cyclones on Modeled Extreme Wind-Wave Climate. *Geophys. Res. Lett.* **2017**, *44*, 1393–1401. [CrossRef]
12. Young, I.R.; Ribal, A. Multiplatform Evaluation of Global Trends in Wind Speed and Wave Height. *Science* **2019**, *364*, 548–552. [CrossRef] [PubMed]
13. Krien, Y.; Dudon, B.; Roger, J.; Arnaud, G.; Zahibo, N. Assessing Storm Surge Hazard and Impact of Sea Level Rise in the Lesser Antilles Case Study of Martinique. *Nat. Hazards Earth Syst. Sci.* **2017**, *17*, 1559–1571. [CrossRef]
14. Rey, T.; Leone, F.; Candela, T.; Belmadani, A.; Palany, P.; Krien, Y.; Cécé, R.; Gherardi, M.; Péroche, M.; Zahibo, N. Coastal Processes and Influence on Damage to Urban Structures during Hurricane Irma (St-Martin & St-Barthélemy, French West Indies). *J. Mar. Sci. Eng.* **2019**, *7*, 215. [CrossRef]
15. Belmadani, A.; Dalphinet, A.; Chauvin, F.; Pilon, R.; Palany, P. Projected Future Changes in Tropical Cyclone-Related Wave Climate in the North Atlantic. *Clim. Dyn.* **2021**, *56*, 3687–3708. [CrossRef]
16. Reguero, B.G.; Méndez, F.J.; Losada, I.J. Variability of Multivariate Wave Climate in Latin America and the Caribbean. *Glob. Planet. Chang.* **2013**, *100*, 70–84. [CrossRef]
17. Morim, J.; Hemer, M.; Wang, X.L.; Cartwright, N.; Trenham, C.; Semedo, A.; Young, I.; Bricheno, L.; Camus, P.; Casas-Prat, M.; et al. Robustness and Uncertainties in Global Multivariate Wind-Wave Climate Projections. *Nat. Clim. Chang.* **2019**, *9*, 711–718. [CrossRef]
18. Hersbach, H.; Bell, B.; Berrisford, P.; Biavati, G.; Horányi, A.; Muñoz Sabater, J.; Nicolas, J.; Peubey, C.; Radu, R.; Rozum, I.; et al. ERA5 hourly data on single levels from 1979 to present. *Copernic. Clim. Change Serv. Clim. Data Store* **2022**. [CrossRef]
19. Hersbach, H.; Bell, B.; Berrisford, P.; Hirahara, S.; Horányi, A.; Muñoz-Sabater, J.; Nicolas, J.; Peubey, C.; Radu, R.; Schepers, D.; et al. The ERA5 Global Reanalysis. *Q. J. R. Meteorol. Soc.* **2020**, *146*, 1999–2049. [CrossRef]
20. Camus, P.; Mendez, F.J.; Medina, R.; Cofiño, A.S. Analysis of Clustering and Selection Algorithms for the Study of Multivariate Wave Climate. *Coast. Eng.* **2011**, *58*, 453–462. [CrossRef]
21. Moron, V.; Gouirand, I.; Taylor, M. Weather Types across the Caribbean Basin and Their Relationship with Rainfall and Sea Surface Temperature. *Clim. Dyn.* **2016**, *47*, 601–621. [CrossRef]
22. Méndez, F.J.; Rueda, A. 3—Wave Climates: Deep Water to Shoaling Zone. In *Sandy Beach Morphodynamics*; Jackson, D.W.T., Short, A.D., Eds.; Elsevier: Amsterdam, The Netherlands, 2020; pp. 39–59. ISBN 978-0-08-102927-5.
23. Dawson, A. Eofs: A Library for EOF Analysis of Meteorological, Oceanographic, and Climate Data. *J. Open Res. Softw.* **2016**, *4*, e14. [CrossRef]
24. Jain, A.K.; Murty, M.N.; Flynn, P.J. Data Clustering: A Review. *ACM Comput. Surv.* **1999**, *31*, 264–323. [CrossRef]
25. Biabiany, E.; Bernard, D.C.; Page, V.; Paugam-Moisy, H. Design of an Expert Distance Metric for Climate Clustering: The Case of Rainfall in the Lesser Antilles. *Comput. Geosci.* **2020**, *145*, 104612. [CrossRef]
26. Arvai, K. K-Means Clustering in Python: A Practical Guide—Real Python. Available online: https://realpython.com/k-means-clustering-python/ (accessed on 17 June 2021).
27. Wang, X.L.; Feng, Y.; Swail, V.R. Changes in Global Ocean Wave Heights as Projected Using Multimodel CMIP5 Simulations. *Geophys. Res. Lett.* **2014**, *41*, 1026–1034. [CrossRef]
28. Naghettini, M. (Ed.) *Fundamentals of Statistical Hydrology*; Springer: Berlin/Heidelberg, Germany, 2016; ISBN 978-3-319-43560-2.
29. Hodges, K.I. Adaptive Constraints for Feature Tracking. *Mon. Weather Rev.* **1999**, *127*, 1362–1373. [CrossRef]
30. Hirsch, M.E.; DeGaetano, A.T.; Colucci, S.J. An East Coast Winter Storm Climatology. *J. Clim.* **2001**, *14*, 882–899. [CrossRef]
31. Paciorek, C.J.; Risbey, J.S.; Ventura, V.; Rosen, R.D. Multiple Indices of Northern Hemisphere Cyclone Activity, Winters 1949–1999. *J. Clim.* **2002**, *15*, 1573–1590. [CrossRef]
32. Eichler, T.; Higgins, W. Climatology and ENSO-Related Variability of North American Extratropical Cyclone Activity. *J. Clim.* **2006**, *19*, 2076–2093. [CrossRef]
33. Hodges, K.I.; Lee, R.W.; Bengtsson, L. A Comparison of Extratropical Cyclones in Recent Reanalyses ERA-Interim, NASA MERRA, NCEP CFSR, and JRA-25. *J. Clim.* **2011**, *24*, 4888–4906. [CrossRef]
34. Bernhardt, J.E.; DeGaetano, A.T. Meteorological Factors Affecting the Speed of Movement and Related Impacts of Extratropical Cyclones along the U.S. East Coast. *Nat. Hazards* **2012**, *61*, 1463–1472. [CrossRef]
35. Booth, J.F.; Rieder, H.E.; Lee, D.E.; Kushnir, Y. The Paths of Extratropical Cyclones Associated with Wintertime High-Wind Events in the Northeastern United States. *J. Appl. Meteorol. Climatol.* **2015**, *54*, 1871–1885. [CrossRef]
36. Varino, F.; Arbogast, P.; Joly, B.; Riviere, G.; Fandeur, M.-L.; Bovy, H.; Granier, J.-B. Northern Hemisphere Extratropical Winter Cyclones Variability over the 20th Century Derived from ERA-20C Reanalysis. *Clim. Dyn.* **2019**, *52*, 1027–1048. [CrossRef]
37. Dodet, G.; Piolle, J.-F.; Quilfen, Y.; Abdalla, S.; Accensi, M.; Ardhuin, F.; Ash, E.; Bidlot, J.-R.; Gommenginger, C.; Marechal, G.; et al. The Sea State CCI Dataset v1: Towards a Sea State Climate Data Record Based on Satellite Observations. *Earth Syst. Sci. Data* **2020**, *12*, 1929–1951. [CrossRef]
38. Timmermans, B.W.; Gommenginger, C.P.; Dodet, G.; Bidlot, J.-R. Global Wave Height Trends and Variability from New Multimission Satellite Altimeter Products, Reanalyses, and Wave Buoys. *Geophys. Res. Lett.* **2020**, *47*, e2019GL086880. [CrossRef]
39. Hurrell, J.W.; Kushnir, Y.; Ottersen, G.; Visbeck, M. An Overview of the North Atlantic Oscillation. In *The North Atlantic Oscillation: Climatic Significance and Environmental Impact*; American Geophysical Union (AGU): Washington, DC, USA, 2003; pp. 1–35, ISBN 978-1-118-66903-7.

40. Morales-Márquez, V.; Orfila, A.; Simarro, G.; Marcos, M. Extreme Waves and Climatic Patterns of Variability in the Eastern North Atlantic and Mediterranean Basins. *Ocean Sci.* **2020**, *16*, 1385–1398. [CrossRef]
41. Lemos, G.; Menendez, M.; Semedo, A.; Miranda, P.M.A.; Hemer, M. On the Decreases in North Atlantic Significant Wave Heights from Climate Projections. *Clim. Dyn.* **2021**, *57*, 2301–2324. [CrossRef]